Electron. Mater. Lett., Vol. 10, No. 4 (2014), pp. 767-773
DOI: 10.1007/s13391-013-3274-0

The Proton Dissociation Constant of Additive Effect on Self-Assembly of Poly(3-hexyl-thiophene) for Organic Solar Cells

Po-Hsun Wang, Hsu-Feng Lee, Yi-Chiang Huang, Yi-Jiun Jung, Fang-Lin Gong, and Wen-Yao Huang*

Department of Photonics, National Sun Yat-Sen University, Kaohsiung 804, Taiwan

(received date: 20 September 2013 / accepted date: 28 October 2013 / published date: 10 July 2014)

In the decision on the pros and cons of the optical and electrical properties of organic solar cells, the morphology has proven to be very important. Easy to change the morphology via adding a small amount of additive, because proton dissociation constant is the main reason for their application. In this study, the use of poly(3-hexylthiophene) and [6,6]-phenyl C_{61}-butyric acid methyl ester as the donor and acceptor materials, and were subsequently doped with different quantity of 4,4'-sulfonyldiphenol, 4,4'-dihydroxybiphenyl, biphenyl-4,4'-dithiol. When the proton dissociation constant is higher and lower respectively, the morphology reveals earthworms-like and fiber-like. For the reason that when the additive is biphenyl-4,4'-dithiol, it can improve the power conversion efficiency of about 27% and the incident photon-to-current conversion efficiency of about 12%.

Keywords: polymer, solar cells, BPDT, BP, BPS, additive

1. INTRODUCTION

Harnessing solar energy is an effective method for dealing with existing energy issues. Currently, photovoltaic (PV) technology is based on inorganic materials, and high material and manufacturing costs have limited its wide acceptance. Intensive research has been conducted toward the development of low-cost PV technologies, among which organic photovoltaic (OPV) devices are some of the most promising. In this region, because of advantages such as affordability, flexibility, and malleability, OPV devices are foremost on many researchers' agendas.[1-12] In past decades, poly(3-hexylthiophene) has been extensively studied as an electron donor material, in combination with fullerene derivatives, such as $PC_{61}BM$ or $PC_{71}BM$, resulting in photoelectric conversion efficiencies (PCEs) of up to 5%.[4-6] Unfortunately, the optical characteristics and defects of the material itself limit its PCE. Several recent studies have been conducted on novel low band gap materials, which capture more solar photons to produce more electron-hole pairs, resulting in improved PCEs of up to 10%.[13-19]

In recent years, the development of new polymer semiconductors and the improved morphology of polymer mixtures have made great progress, which has had a major influence on photo-physical and organic solar cells. Optimizing polymer solar cell processing conditions, which include methods such as heat hardening, solvent selection, solvent-assisted thermal training, nano-fiber mixing, sol-gel assisted methods, and solvent and surfactant additives, significantly improves the PCEs of OPV devices.[2,3,7,10,13,20-24] However, these techniques can affect the polymer blend in micro-phase separation and ordination, allowing the formation of a donor and acceptor-type ordered interpenetrating network; the end goal is the formation of nano-scale micro-phase separation of pairs in a continuous phase. Often, a good choice of donor material for obtaining optimal carrier generation and transmission and for improving the absorption of light in crystalline type polymer semiconductors is poly(3-hexylthiophene). In order to fabricate an ideal crystal type polymer semiconductor, previous research indicates that the surfactant is the most important component to modify.

In their research, Bazan *et al.* first reported a significant PCE improvement to higher than 5% in $PC_{71}BM$ blends of a low band gap polymer poly[2,6-(4,4-bis(2-ethylhexyl)-4H-cyclopenta[2,1-b;3,4-b0]dithiophene)-alt-4,7-(2,1,3-benzothiadiazole)] (PCPDTBT) upon the addition of a few volume percent of either alkanedithiols or alkanedihalides.[5,25] Shortly thereafter, the Lam[26] team further added to a series of different alkyl chain lengths of alkanedithiols in the active layer, and explored the influence of the alkyl chain length on the hybrid morphology of the active layer and the PCE. The previous literature discusses this structure because it has a thiol functional group, which drives the self-assembly of the P3HT assistant. 1,8-octanedithol is a good crystallization accelerator, not only increasing the crystallinity of P3HT, but also allowing it to obtain more sunlight. However, we think that thiol does not major factor, and instead the proton-donating ability.[27,28] On the P3HT

*Corresponding author: wyhuang@mail.nsysu.edu.tw

molecule, the thiophene derivative because of the sulfur atom in the thiophene ring with the electropositive characteristics of the relationship, therefore easy nucleophilic doping.[29-31] Because of the additive dissociated hydrogen ions in the solvent, it can reduce the distance between the molecules. For research on this feature, a series of acid dissociation constants of additives will be discussed. The present study is the first to propose biphenyl-4,4'-dithiol (BPDT), 4,4'-dihydroxybiphenyl (BP), 4,4'-sulfonyldiphenol (BPS), as surfactant additives with the composite P3HT/PCBM. This series of additives, because of their different groups, have different proton-donating ability, and will directly influence the morphology of the molecular arrangement, improving the PCE.

2. EXPERIMENTAL PROCEDURE

Electron donor material P3HT and electron acceptor $PC_{61}BM$ were purchased from Luminescence Technology Corp., and used as received. The BPDT, BP, and BPS was purchased from Aldrich, Alfa Aesar, and TCI-EP, respectively. The PEDOT:PSS (483095) was obtained from Aldrich. The sheet resistance and thickness of the ITO glass substrate were 5 Ω/□ and 280 nm respectively. Photo-lithography was used to define the anode plot. The glass substrate was then placed within an ultrasound washer, in sequence using acetone, methyl alcohol and deionized water each for 8 minutes. The glass substrate was then blown dry by nitrogen and placed in an oven for 8 minutes. The surface of the ITO glass was cleaned in an oxygen plasma environment, and that was then removed and spin coated a layer of PEDOT:PSS. In the atmospheric environment, the active layer material (P3HT:PCBM = 1:1) was dissolved in chlorobenzene (CB) to form a 1.7 wt. % solution and then placed on a hot plate at temperature 40°C, stirring at 200 rpm for 24 hours; the P3HT:PCBM solution was then spin coated on the PEDOT:PSS layer. For regular devices, an active layer was spin-cast on the ITO/PEDOT:PSS, then dried on a hot-plate at 130°C. A 0.2 nm LiF layer and a 90 nm Al layer were subsequently evaporated through a shadow mask to define the active area of the devices (0.09 cm^2) and form a top anode. Under the experimental details, the device fabrication is not optimal. The PCE values were determined from *J-V* curve measurements (using a Keithley 2400 source meter) under a 1 sun, AM 1.5G spectrum from a solar simulator (1000 W m^{-2}).

The dissociation constant for this equilibrium is defined as:

$$K_a = \frac{[H_3O^+][A^-]}{[HA]}.$$

Strong acids are dissociated in aqueous solution and their K_a is high. The acids that donate more than one proton have a specific acid constant related to ionization. In this condition, we can define the acid pK_a as the logarithm of inverse K_a:

$$pK_a = -\log K_a = \log\left(\frac{1}{K_a}\right).$$

3. RESULTS AND DISCUSSION

3.1 Analysis of film properties

As shown in the chemical structures in Figs. 1(a)-(c), we proposed a series of acid dissociation constants of different additives: biphenyl-4,4'-dithiol (BPDT), 4,4-dihydroxybiphenyl (BP), and 4,4'-sulfonyldiphenol (BPS) of pK_a 9.63, 9.28, and 8, respectively, as provided by the material supplier.

Figure 2 shows the respective x-ray diffraction spectra for the BPDT, BP, and BPS, added to the P3HT/PCBM blend. The results show a diffraction angle of approximately 5.2 degrees, and all spectra have strong diffraction peaks. The results of the XRD denote the volume fraction of the p-conjugated planes of P3HT (100) with lamella oriented normal to the substrate.[32,33] In general, the solvent additives should have higher boiling point and selectively solubility to one BHJ component.[6,25,26] However, that hydrogen or ionic bonds is likely to be affected causes. Furthermore, the hydrogen ions will be induced to form chemical bonds.[28] In this series of additives, the diffraction peak increases as the doping concentration increases. The information indirectly tells us that the dissociated hydrogen ions of the additives affect the amount of diffracted intensity, which leads to changes in the crystallinity of P3HT. An increase in additive concentration means that there are more hydrogen ions to dissociate. The additives obtained their strongest diffraction peaks when concentrations were 0.12, 0.72, and 0.07 wt. %, respectively. Since the resultant hydrogen ions at these concentrations enhanced the intermolecular forces in

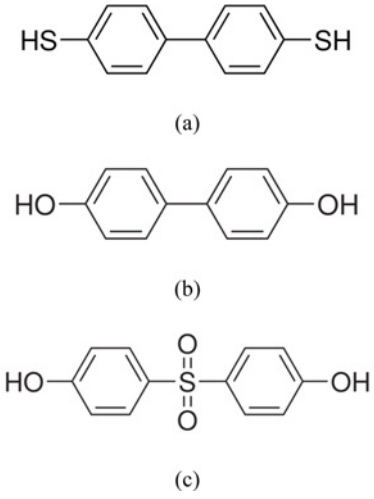

Fig. 1. The chemical structures of (a) biphenyl-4,4'-dithiol, (b) 4,4'-dihydroxybiphenyl, and (c) 4,4'-sulfonyldiphenol.

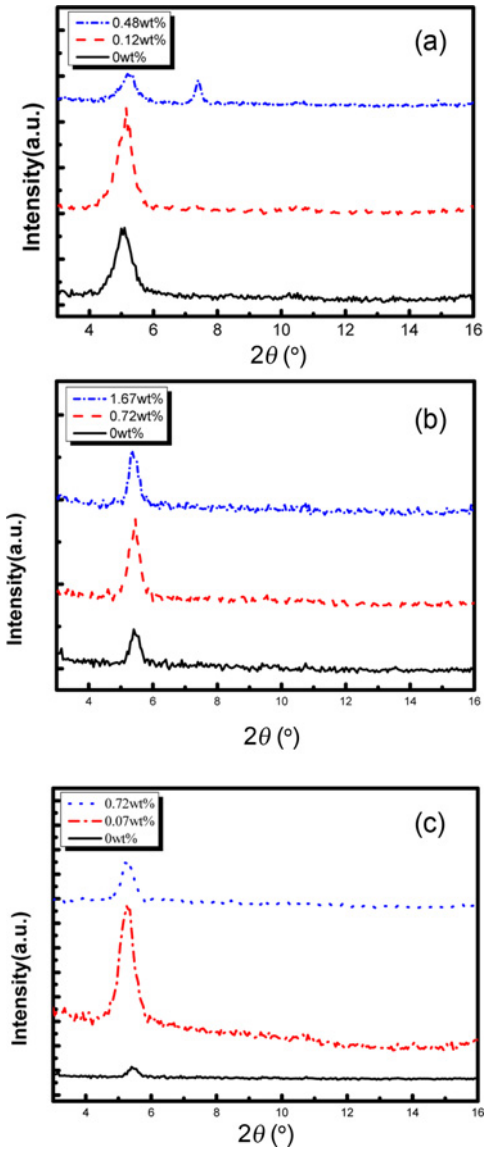

Fig. 2. X-ray diffraction measurement of P3HT:$PC_{61}BM$ blends with different concentration of (a) biphenyl-4,4'-dithiol, (b) 4,4'-dihydroxybiphenyl, and (c) 4,4'-sulfonyldiphenol.

P3HT,[34,35] the crystallinities of the P3HTs were improved. Furthermore, this reason reveal that poly(3-hexylthiophene) separate out with hydrochloric acid, which is under synthetic process. However, it was noted that when the doping concentrations of these additives were 0.48, 1.67, and 0.72 wt. %, since the doping additive was in excess, the arrangement of the P3HTs were disrupted, causing a decrease in the diffraction peak intensities. When the amount of the doping additive reached a certain degree of excess, other diffraction peaks were generated; we observed this phenomenon at 0.48 wt. %.

When the excess doping amount was located in the $2\theta = 5\sim6$ degree range of the diffraction peak, the intensity decreased. Additionally, another diffraction peak was produced at $2\theta = 7.39$ degrees. We can speculate that excessive doping additives may form the unknown complex which include additives and donor/accepter material. The results may be produced another diffraction peak, and caused by a mixture of the formation of a more substantial phase separation. However, other additives did not exhibit this phenomenon, presumably as they had not yet reached their excess limits; this will be confirmed in subsequent transmission electron microscopy (TEM) analysis. Moreover, the α-axis direction refers to the P3HT chain parallel to the vertical distance of the side chain. Therefore, Bragg's formula is used to calculate the molecular distance of $2\theta = 5\sim6$ degrees of P3HT molecules of crystallization at (100) crystal planes of the α-axis direction, as shown in Table 1.

In the P3HT/PCBM blends, regardless of the doping concentration of the additives, the distance between the molecules was only slightly changed for 0.5 Å. However, in this small amplitude variation, we hypothesized that the effective conjugation length of the polymer will thus be changed. In past research, the Raman spectroscopy technique was often used to identify conjugated polymer conjugation length variations in the effective techniques. Therefore, in this study, we used Raman spectroscopy to measure and analyze the blends. As shown in Fig. S2 and Table 1, in this

Table 1. The film properties of the P3HT/$PC_{61}BM$ fabricated with various processing additives.

Additive	Concentration (wt. %)	Absorbance Max intensity	XRD		Raman Wavenumber (cm^{-1})
			2θ	d (Å)	
BPDT	0	503 nm	5.10	17.3	1447
-	0.12	507 nm	5.15	17.1	1442
-	0.48	491 nm	5.2/7.39	17.1/11.9	1446
BP	0	503 nm	5.40	16.35	1446.5
-	0.72	503 nm	5.44	16.23	1447.9
-	1.67	503 nm	5.3	16.67	1446.8
BPS	0	503 nm	5.39	16.38	1446.45
-	0.07	510 nm	5.25	16.81	1446.11
-	0.72	506 nm	5.19	16.92	1448.13

series of additives for optimal doping concentration, when the additives were BPDT, BP, and BPS, the signal peaks compared with undoped films, showing a blue shift, red shift, and blue shift. According to the literature, these signal peaks represent C=C of the stretching signal of P3HT. When this signal peak red shifts, the results represent higher and localization of electron density on the C=C, and the effective conjugate length decreases, while the relative intensity of the stretching peak for the C=C enhancement representing the crystal film is improved. Therefore, because of the dissociated hydrogen ions of the additives, resulting in intermolecular force changes, there is a small change in the effective conjugation lengths.

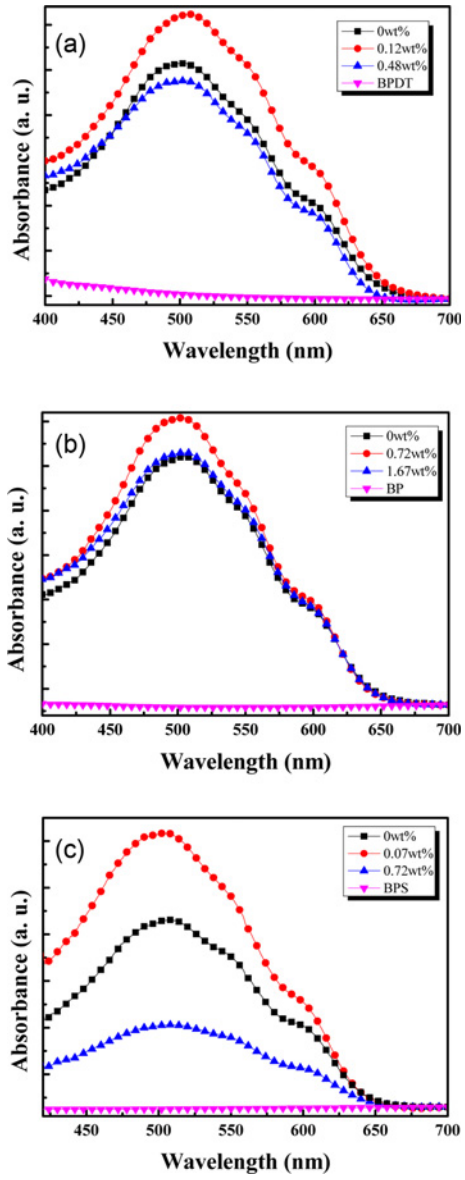

Fig. 3. The UV-Vis for P3HT:$PC_{61}BM$ blends with (a) biphenyl-4,4'-dithiol, (b) 4,4'-dihydroxybiphenyl, and (c) 4,4'-sulfonyldiphenol of additive. (The curves normalized to the film thicknesses).

These slight changes in the blends directly influence the absorption of sunlight. Figure 3 depicts the UV-Vis absorption spectra for the P3HT/PCBM blends. First, in the visible wavelength of 430 nm to 700 nm, the additives do not absorb any light. When there is no doping additive, the maximum absorption wavelength of 503 nm is considered the standard device. When the doping concentration of BPDT is 0.12 wt. %, the maximum absorption wavelength red shifts to 507 nm. When the doping concentration of BP is 0.72 wt. %, the maximum absorption wavelength blue shifts to 503 nm. When the doping concentration of BPS is 0.07 wt. %, the maximum absorption wavelength red shifts to 510 nm. In this regard, many similar studies have shown that the absorption band around 503 nm is the absorption of the P3HT π-π^* transition.[36] With a small amount of doping additive, it is obvious that the maximum absorption peak has a slight red shift, and the absorption coefficient of the blends is enhanced at wavelengths of 430 to 700 nm. This is maybe because the additive dissociated hydrogen ions in the blends affect the P3HT intermolecular force, resulting in slight improvement in the effective conjugation length and the distance between the P3HT molecules, thus promoting regular arrangement of P3HT molecules. However, not only will doping with excessive additives cause the wavelength of the maximum absorption peak to blue shift, it will also result in weakening of the absorption coefficient. This phenomenon is due to an excessive amount of additives, which obstructs the arrangement. This phenomenon leads to π-π^* transition of weakening, while arranging the P3HT molecules to form different patterns, which results in blue shifting of the absorption band and a decrease in the coefficient.

We will also focus on the maximum diffraction peak of each additive, when the pK_a is 9.63 with a smaller diffraction peak. As the pK_a decreased, the diffraction intensity increased. The largest diffraction peak occurred when the pK_a was 8. Previous research indicates that blends must form a nano-scale micro-phase separation. Because of PCBM, P3HT also affects the nature of the ideal arrangement, resulting in reduced diffraction intensity in P3HT. Therefore, when the pK_a value is greater, the arrangement type of P3HT is enhanced. When the pK_a value is smaller, P3HT has a relatively inferior arrangement type. But in order to form a micro-phase separation, P3HT and PCBM must be complementary. So in order to understand the acid dissociation constants for the micro-structure effects, we used TEM in this study to identify and analyze surface micro-structure. Figure 4 shows the best doping concentration conditions, when the pK_a is 9.63 and the surface shows an earthworm-like morphology; when the pK_a is 8, the surface morphology shows a fiber-like morphology; when the pK_a is 9.28, the surface morphology shows a transitional phenomenon between earthworm-like and fiber-like. In addition, an excess of doping additives leads to the destruction of the micro-phase separated blends.

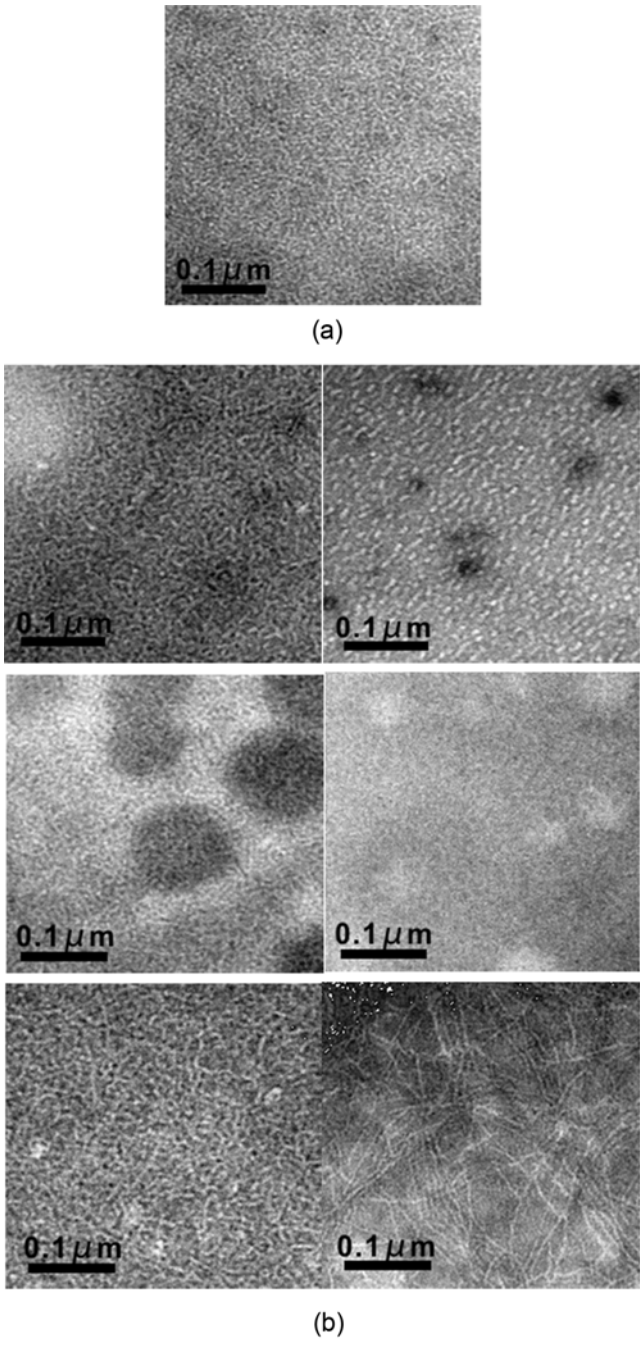

Fig. 4. (a) The transmission electron microscopy for P3HT:$PC_{61}BM$ blends without additive, and (b) with biphenyl-4,4'-dithiol (top), 4,4'-dihydroxybiphenyl (middle), 4,4'-sulfonyldiphenol (bottom) of additive.

3.2 Measurement of the optical and electrical properties

Different acid dissociation constants result in different types of surface morphologies; therefore, different forms of surface morphology are applied to polymer solar cells. Figure 5 shows the Incident photon-to-current conversion efficiency (IPCE) results of photovoltaic cells fabricated

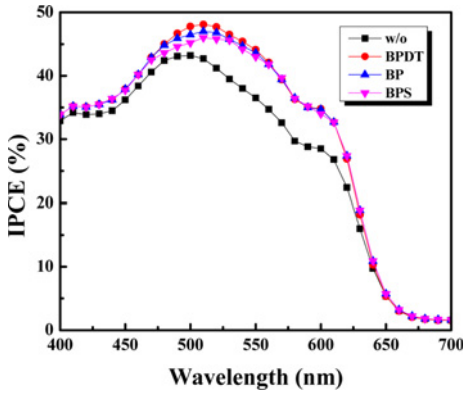

Fig. 5. The Incident photon-to-current conversion efficiency (IPCE) of P3HT:$PC_{61}BM$ blends with different additives.

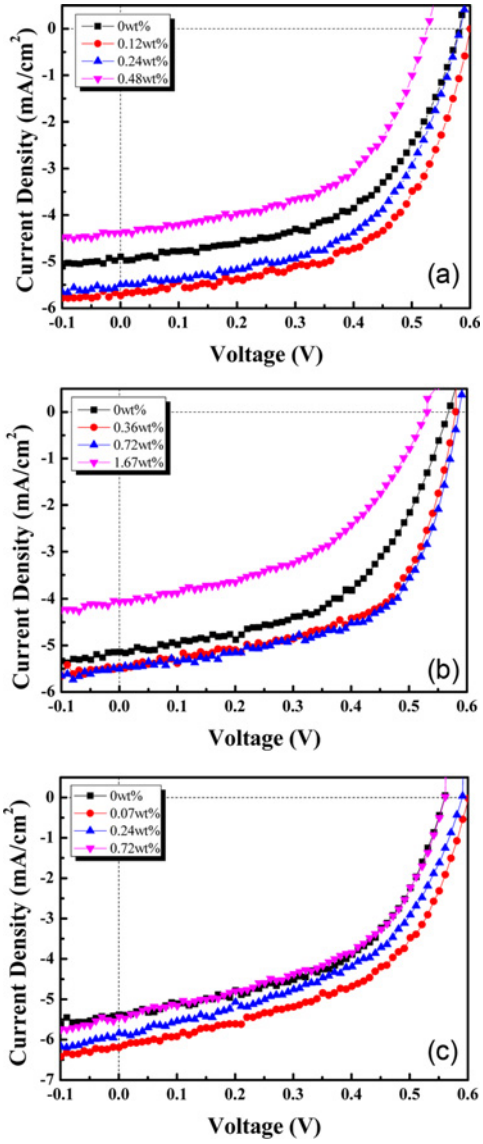

Fig. 6. The current density-voltage (*J-V*) characteristics of P3HT:$PC_{61}BM$ blends with different concentration of (a) biphenyl-4,4'-dithiol, (b) 4,4'-dihydroxybiphenyl, and (c) 4,4'-sulfonyldiphenol.

Table 2. Photovoltaic performances of the BHJ polymer solar cells composed P3HT/$PC_{61}BM$ fabricated with various processing additives.

Additive	Concentration (wt. %)	V_{oc} (V)	J_{sc} (mA/cm^2)	FF	PCE (%)	Rs (Ω-cm)	Rsh (Ω-cm)
BPDT	0	0.58	4.90	0.54	1.54	11.85	839.69
-	0.12	0.60	5.73	0.57	1.95	7.17	963.23
-	0.48	0.53	4.38	0.53	1.24	8.73	808.41
BP	0	0.57	5.14	0.52	1.53	9.38	699.22
-	0.72	0.58	5.46	0.59	1.92	5.01	803.21
-	1.67	0.53	4.07	0.48	1.03	9.07	674.78
BPS	0	0.56	5.38	0.51	1.56	6.56	432.67
-	0.07	0.60	6.20	0.52	1.92	6.25	603.58
-	0.72	0.57	3.54	0.37	0.75	16.56	432.79

with difference additive. The IPCE maximum of 42.7% at 500 nm was observed for P3HT:PCBM. The IPCE maximum of 48%, 47% and 46% at 510 nm was observed for P3HT:PCBM with BPDT, BP and BPS respectively. The IPCE of photovoltaic cells was observed to enhance at 530 nm by doping additive, due to enhanced the intermolecular forces in P3HT. Figure 6 shows the *J-V* characteristics of doped with different amounts of additive mapping, and the optical characteristics are compiled in Table 2. With the best concentrations, the optical and electrical properties of the respective additives will be because P3HT has good crystallinity, allowing excellent light absorption, and providing the highest short-circuit current and PCE. However, excess dopant destroys the morphology, which increases the series resistance and decreases the shunt resistance. Furthermore, with optimal concentrations, the pK_a were 9.63, 9.28, and 8, and the PCE compared to un-doped device, was improved by 27, 25, and 23%, respectively. Therefore, when the pK_a is 9.63, although the arrangement of P3HT is relatively poor, the micro-phase separation results in excellent PCE. Conversely, a decreased acid dissociation constants results in the destruction of good micro-phase separation.

4. CONCLUSIONS

Through the process of the active layer is doped with additives, we demonstrate that the proton-donating ability is the reason for the influence of the organic solar cell efficiency. As we appropriate doping additives, will make excellent micro-phase separation between the P3HT and PCBM. The reason maybe is that hydrogen ions will be influenced the arrangement by the intermolecular force. Thus, it is fine-tuning for the distance between P3HTs. So, the molecules of P3HT can reach thermodynamic equilibrium of regularly arranged. The surface morphology of the P3HT/PCBM blends, in the higher pK_a value, is showing an earthworms-like morphology. In the lower pK_a value, showing a fiber-like morphology. And in the optical characteristics of the presentation, when the pK_a value of 9.63, although the arrangement of P3HT is relatively poor, but this time showing a good nano-scale phase separation, so that the PCE was improved by 27%. When the pK_a of 8, although the arrangement of P3HT is less excellent, but it destroyed a good micro-phase separation, so that the PCE was improved by 23%. In addition, the acid dissociation constants under the middle value, the PCE is improved by 25%. However, the proton-donating ability is not absolute under technology, which is solvent additive. Until now, we can't identify clearly the main reason. But, we can determine the reason, which is include the hydrogen and ionic bonds. The results improve the absorption of sunlight and the carrier transport, and reduce the internal resistance of the blends.

ACKNOWLEDGMENTS

This project was supported by the National Science Council for the funding of this project No. NSC-100-2221-E-110-046. Moreover, I thank that Professor J.S. Huang of National Cheng Kung University supplies the Raman analytical instruments measurement.

REFERENCES

1. B. C. Thompson and J. M. J. Frechet, *Angew. Chem., Int. Ed.* **47**, 58 (2008).
2. G. Dennler, M. C. Scharber, and C. J. Brabec, *Adv. Mater.* **21**, 1323 (2009).
3. L.-M. Chen, Z. Hong, G. Li, and Y. Yang, *Adv. Mater.* **21**, 1434 (2009).
4. Y. Yao, J. Hou, Z. Xu, G. Li, and Y. Yang, *Adv. Funct. Mater.* **18**, 1783 (2008).
5. W. Ma, C. Yang, X. Gong, K. Lee, and A. J. Heeger, *Adv. Funct. Mater.* **15**, 1617 (2005).
6. J. Peet, J. Y. Kim, N. E. Coates, W. L. Ma, D. Moses, A. J. Heeger, and G. C. Bazan, *Nat. Mater.* **6**, 497 (2007).
7. G. Li, V. Shrotriya, J. Huang, Y. Yao, T. Moriarty, K. Emery, and Y. Yang, *Nat. Mater.* **4**, 864 (2005).
8. Z. He, C. Zhong, S. Su, M. Xu, H. Wu, and Y. Cao, *Nat.*

Photonics **6**, 591 (2012).
9. M. Kaltenbrunner, M. S. White, E. D. Gtowacki, T. Sekitani, T. Someya, N. Sariciftci, and S. Bauer, *Nat. Commun.* **3**, 770 (2012).
10. Y. S. Tsai, J.-S. Lin, W.-P. Chu, P.-H. Wang, F.-S. Juang, M.-H. Chung, C.-M. Chen, and M. O. Liu, *Curr. Appl. Phys.* **10**, S502 (2010).
11. W. Y. Huang, C. C. Lee, S. G. Wang, Y. K. Han, and M. Y. Chang, *J. Electrochem. Soc.* **157**, B1336 (2010).
12. W. Y. Huang, C. C. Lee, and T. L. Hsieh, *Sol. Energ. Mat. Sol. C.* **93**, 382 (2009).
13. Y. Liang, Z. Xu, J. Xia, S.-T. Tsai, Y. Wu, G. Li, C. Ray, and L. Yu, *Adv. Mater.* **22**, E135 (2010).
14. T.-Y. Chu, J. Lu, S. Beaupr, Y. Zhang, J.-R. Pouliot, S. Wakim, J. Zhou, M. Leclerc, Z. Li, J. Ding, and Y. Tao, *J. Am. Chem. Soc.* **133**, 4250 (2011).
15. J. H. Seo, A. Gutacker, Y. Sun, H. Wu, F. Huang, Y. Cao, U. Scherf, A. J. Heeger, and G. C. Bazan, *J. Am. Chem. Soc.* **133**, 8416 (2011).
16. Y. Liu, Y. (Michael) Yang, C.-C. Chen, Q. Chen, L. Dou, Z. Hong, G. Li, and Y. Yang, *Adv. Mater.* **25**, 4657 (2013).
17. L. Dou, C.-C. Chen, K. Yoshimura, K. Ohya, W.-H. Chang, J. Gao, Y. Liu, E. Richard, and Y. Yang, *Macromolecules* **46**, 3384 (2013).
18. J. You, C.-C. Chen, Z. Hong, K. Yoshimura, K. Ohya, R. X. S. Ye, J. Gao, G. Li, Y. Yang, *Adv. Mater.* **25**, 3973 (2013).
19. S. A. Hawks, F. Deledalle, J. Yao, D. G. Rebois, G. Li, J. Nelson, Y. Yang, T. Kirchartz, and J. R. Durrant, *Adv. Energy Mater.* **3**, 1201 (2013).
20. P. E. Keivanidis, T. M. Clarke, S. Lilliu, T. Agostinelli, J. E. Macdonald, J. R. Durrant, D. D. C. Bradley, and J. Nelson, *J. Phys. Chem. Lett.* **1**, 734 (2010).
21. M. F. G. Klein, F. M. Pasker, S. Kowarik, D. Landerer, M. Pfa, M. Isen, D. Gerthsen, U. Lemmer, S. Hoger, and A. Colsmann, *Macromolecules* **46**, 3870 (2013).
22. H.-Y. Chen, H. Yang, G. Yang, S. Sista, R. Zadoyan, G. Li, and Y. Yang, *J. Phys. Chem. C* **113**, 7946 (2009).
23. T. L. Andrew and V. Bulovic, *ACS Nano* **6**, 4671 (2012).
24. E. Wang, Z. Ma, Z. Zhang, K. V., P. Henriksson, O. Inganas, F. Zhang, and M. R. Andersson, *J. Am. Chem. Soc.* **133**, 14244 (2011).
25. J. K. Lee, W. L. Ma, C. J. Brabec, J. Yuen, J. S. Moon, J. Y. Kim, K. Lee, G. C. Bazan, and A. J. Heeger, *J. Am. Chem. Soc.* **130**, 3619 (2008).
26. T. Salim, L. H. Wong, B. Brauer, R. Kukreja, Y. L. Foo, Z. Bao, and Y. M. Lam, *J. Mater. Chem.* **21**, 242 (2011).
27. M. T. Lee, C. K. Yen, W. P. Yang, H. H. Chen, C. H. Liao, C. H. Tsai, and C. H. Chen, *Org. Lett.* **6**, 1241 (2004).
28. W.-T. Liu, P.-H. Wang, H.-F. Lee, Y.-C. Huang, and W.-Y. Huang, *J. Solid State Sci. Tech.* **2**, R142 (2013).
29. Z. Liang, M. O. Reese, and B. A. Gregg, *ACS Appl. Mater. Interfaces* **3**, 2042 (2011).
30. K. Geramita, Y. Tao, R. A. Segalman, and T. D. Tilley, *J. Org. Chem.* **75**, 1871 (2010).
31. Y. Li, K. Kamata, S. Asaoka, T. Yamagishi, and T. Iyoda, *Org. Biomol. Chem.* **1**, 1779 (2003).
32. G. Li, Y. Yao, H. Yang, V. Shirotriya, G. Yang, and Y. Yang, *Adv. Funct. Mater.* **17**, 1636 (2007).
33. Y. Kim, S. Cook, S. M. Tuladhar, S. A. Choulis, J. Nelson, J. R. Durrant, D. D. C. Bradley, M. Giles, I. Mcculloch, C.-S. Ha, and M. Ree, *Nat. Mater.* **5**, 197 (2006).
34. P. J. Brown, D. S. Thomas, A. Kohler, J. S. Wilson, J. -S. Kim, C. M. Ramsdale, H. Sirringhaus, and R. H. Friend, *Phys. Rev. B* **67**, 064203-1 (2003).
35. T.-Q. Nguyen, R. C. Kwong, M. E. Thompson, and B. J. Schwartz, *Appl. Phys. Lett*. **76**, 2454 (2000).
36. E. M. Conwell, C. B. Duke, A. Paton, and S. Jeyadev, *J. Chem. Phys.* **88**, 3331 (1988).